Heung Fai Lam, Ching Tai Ng and Andrew Yee Tak Leung
Multicrack detection on semirigidly connected beams utilizing dynamic data
Journal of Engineering Mechanics-ASCE, 2008; 134(1):90-99

DOI: 10.1061/(ASCE)0733-9399(2008)134:1(90)

Submitted to the Journal of Engineering Mechanics, ASCE (July 2006)

Multi-Crack Detection on Semi-Rigidly Connected Beams Utilizing Dynamic Data

Heung Fai LAM[+] and Ching Tai NG

Department of Building and Construction, City University of Hong Kong, Kowloon Tong, Kowloon, Hong Kong

[+] send correspondence to Dr HF Lam (paullam@cityu.edu.hk)

Keywords: Bayesian model class selection; Bayesian statistical framework; Semi-rigid connection; Crack detection; Modeling error; Measurement noise.

Total no. of pages: 21 (text, including this page) + 9 (figures) + 10 (tables) = 40

Multi-Crack Detection on Semi-Rigidly Connected Beams Utilizing Dynamic Data

Heung Fai LAM[1] and Ching Tai NG[2]

Abstract

The problem of crack detection has been studied by many researchers, and many methods of approaching the problem have been developed. To quantify the crack extent, most methods follow the model updating approach. This approach treats the crack location and extent as model parameters, which are then identified by minimizing the discrepancy between the modeled and the measured dynamic responses. Most methods following this approach focus on the detection of single-crack or multi-crack in situations in which the number of cracks is known. The main objective of this paper is to address the crack detection problem in a general situation in which the number of cracks is not known in advance.

The crack detection methodology proposed in this paper consists of two phases. In the first phase, different classes of models are employed to model the beam with different numbers of cracks, and the Bayesian model class selection method is then employed to identify the most plausible class of models based on the set of measured dynamic data in order to identify the number of cracks on the beam. In the second phase, the posterior (updated) probability density function (PDF) of the crack locations and the corresponding extents is calculated using the Bayesian statistical framework. As a result, the uncertainties that may have been introduced by measurement noise and modeling error can be explicitly dealt with.

The methodology proposed herein has been verified by and demonstrated through a comprehensive series of numerical case studies, in which noisy data was generated by a Bernoulli-Euler beam with semi-rigid connections. The results of these studies show that the proposed methodology can correctly identify the number of cracks even when the crack extent is small. The effects of measurement noise, modeling error, and the complexity of the class of identification model on the crack detection results have also been studied and are discussed in this paper.

[1] Assistant Professor, Department of Building and Construction, City University of Hong Kong. Email: paullam@cityu.edu.hk. [Corresponding author]
[2] Research Student, Department of Building and Construction, City University of Hong Kong. Email: 50410377@student.cityu.edu.hk.

1 Introduction

The problem of crack detection has been studied by many researchers, and many methods following different approaches and based on different assumptions have been developed. A comprehensive review of recent developments can be found in Sohn *et al*. (2004). Most of the crack detection methods in the literature have focused on single-crack cases (Cawley & Adams 1979; Rizos *et al.* 1990; Liang *et al.* 1991; Narkis 1994; Nandwana & Maiti 1997). For methods that have addressed multi-crack situations, it has been assumed that the number of cracks was known in advance. Ostachowicz and Krawczuk (1991) studied the forward problem of a beam structure with two cracks. They expressed the changes in dynamic behavior as a function of crack location and extent. Ruotolo and Surace (1997) studied the inverse problem of the crack detection of beam structures utilizing natural frequencies and mode shapes. They formulated the crack detection process (estimating the location and extent of cracks) as an optimization problem, and solved it by genetic algorithm when the number of cracks was known. Similarly, Law and Lu (2005) proposed the use of measured time-domain responses in the detection of a given number of cracks on a beam structure through optimization algorithms. The difficulty with this method is that the number of cracks on a beam is generally not known before crack detection.

Lam *et al.* (2005) studied the use of spatial wavelet transform in the detection of the crack location and extent of an obstructed beam using the Bayesian probabilistic framework in which there is only one crack on the structural member. One of the objectives of this paper is to extend the work of Lam *et al.* (2005) to the multi-crack cases in which the number of cracks is not known in advance. The crack detection methodology proposed here is divided into two phases. In the first phase, the Bayesian model class selection method (Beck & Yuen 2004) is employed to identify the number of cracks based on a given set of measured dynamic data. Once the number of cracks has been identified, the posterior probability density function (PDF) of the locations and extents of the cracks are then calculated using the Bayesian statistical framework (Beck & Katafygiotis 1998) in the second phase. Unlike the deterministic approach, which focuses on pinpointing crack locations and extents, the objective of the crack detection methodology proposed in this paper is to calculate the posterior (or updated) probability density function (PDF) of the crack locations and extents. The PDF conveys valuable information to engineers about the confidence level of the crack detection results.

The organization of this paper is as follows. In Section 2, the proposed methodology is

presented and the related background theories, such as the modeling of the cracked beam, the Bayesian model class selection, and the Bayesian statistical framework, are reviewed. Section 3 reports the results of a series of comprehensive numerical case studies, which verify and demonstrate the proposed crack detection methodology. The effects of measurement noise, modeling error, and the complexity of the class of identification model on the results of crack detection are then discussed, based on the results of these case studies. Conclusions are drawn at the end of the paper.

2 Proposed Methodology and Background Theories

The proposed crack detection methodology consists of two phases. The number of cracks is identified in the first phase and the PDF of crack location and extent is calculated in the second phase.

The basic strategy in the first phase is to adopt different classes of models for beams with different numbers of cracks (see Figure 1) and to identify the "best" model class based on a set of dynamic measurement D following the Bayesian model class selection method (Beck & Yuen 2004). In Figure 1, the model class M_j is employed in modeling a beam with *j* cracks for $j = 0,\ldots,N_M$, where N_M is the maximum number of cracks to be considered in the crack detection process, and the parameters l_j and Δ_j are used to describe the location and extent of the *j*th crack.

It must be pointed out that the selection of the "best" model class based on a given set of data is not trivial. It is clear that the model class of a beam with more cracks consists of more model parameters (e.g., M_2 has two additional model parameters l_2 and Δ_2 when compared to M_1 as shown in Figure 1). A model class with more parameters will always provide a better fit to the measurement when compared to a model class with fewer parameters. Consider a double-crack case as an example: in the presence of measurement noise, the optimal model in the 3-crack model class (M_3) will fit the measurement better than that in the 2-crack model class (M_2), as the additional parameters l_3 and Δ_3 in M_3 can be used to compensate for the effect of measurement noise. In the extreme situation of selecting an M_3-model (i.e., a model in the model class M_3) with $\Delta_3 = 0$ and other parameters the same as in those of the optimal M_2-model (l_3 can take any value when Δ_3 is equal to zero), this M_3-model can fit

the measurement as well as the optimal M_2-model. Therefore, the selection of model class based solely on the fitting between the modeled and the measured dynamic responses can be very misleading, as the most complex model class will always be selected. In this paper, the Bayesian model class selection method is employed in choosing the "best" class of models based on a given set of data for the purpose of identifying the number of cracks. A brief review of the Bayesian model class selection method is presented in Section 2.2.

In the second phase of the methodology, the posterior PDF of the crack locations and the corresponding extents are calculated following the Bayesian statistical framework (Beck & Katafygiotis 1998), which is briefly reviewed in Section 2.3. The following section covers details concerning the modeling of a beam with multiple cracks.

2.1 Modeling and parameterization of cracked beams

For an Bernoulli-Euler beam, the governing equation of motion under free vibration is:

$$EI\frac{\partial^4 y(x,t)}{\partial x^4}+m\frac{\partial^2 y(x,t)}{\partial t^2}=0 \tag{1}$$

where EI is the flexural rigidity; m is the mass density (mass per unit length); and y is the transverse deflection of the beam. By separation of variables $y(x,t)=\phi(x)z(t)$, the displacement $y(x,t)$ can be separate as the modal amplitude $z(t)$ and the mode shape function $\phi(x)$. Thus, the mode shape function is:

$$\frac{d^4\phi(x)}{dx^4}-\beta^4\phi(x)=0 \tag{2}$$

where $\beta^4=\omega^2 m/EI$; and ω is the angular natural frequency of the system in radians per second.

Formatted

Figure 2

Formatted
spelling or

~~Figure 2~~ shows the model of a beam with N_C cracks. The beam is divided into N_C+1 segments, each with length l_i, for $i=1,\ldots,N_C+1$, where $\sum_{i=1}^{N_C+1} l_i = L$. The segments are connected at the crack locations through mass-less rotational springs. The general solution of the ϕ function for each segment can be expressed as:

$$\phi_i(x_i)=A_i\sin(\beta x_i)+B_i\sinh(\beta x_i)+C_i\cos(\beta x_i)+D_i\cosh(\beta x_i) \tag{3}$$

where $i=1,\ldots,N_C+1$; A_i, B_i, C_i and D_i are unknown coefficients to be calculated from boundary and continuity conditions. The four boundary conditions are:

$$\begin{aligned}
&\phi_1(0) = \phi_{N_C+1}\left(l_{N_C+1}\right) = 0 \\
&K_L \frac{d\phi_1(0)}{dx} = EI \frac{d^2\phi_1(0)}{dx^2} \\
&K_R \frac{d\phi_{N_C+1}\left(l_{N_C+1}\right)}{dx} = EI \frac{d^2\phi_{N_C+1}\left(l_{N_C+1}\right)}{dx^2}
\end{aligned} \tag{4}$$

where K_L and K_R are the stiffness coefficients of the rotational springs at the left and right ends of the beam respectively. The rotational springs model the semi-rigid behavior of the beam end connections (Chen & Kishi 1989). At the general *i*th segment of the beam, the following four continuity conditions must be satisfied:

$$\begin{aligned}
&\phi_i(l_i) = \phi_{i+1}(0) \\
&\frac{d\phi_{i+1}(0)}{dx} - \frac{d\phi_i(l_i)}{dx} = \Delta_i L \frac{d^2\phi_{i+1}(0)}{dx^2} \\
&\frac{d^2\phi_i(l_i)}{dx^2} = \frac{d^2\phi_{i+1}(0)}{dx^2} \\
&\frac{d^3\phi_i(l_i)}{dx^3} = \frac{d^3\phi_{i+1}(0)}{dx^3}
\end{aligned} \tag{5}$$

where $i = 1, ..., N_C$; Δ_i is the non-dimensional flexibility parameter to characterize the extent of the *i*th crack. The relationship between the crack extent Δ_i and the crack depth ratio $\delta_i = a_i / h$ can be found in Ostachowicz *et al.* (1991) as:

$$\Delta_i = 6\pi\delta_i^2 \left(\frac{h}{L}\right) f(\delta_i) \tag{6}$$

where h is the beam depth; a_i is the depth of the *i*th crack (see Figure 2~~Figure 2~~); and the function $f(\delta_i)$ is given by:

Formatted

Formatted
spelling or

$$f(\delta_i) = 0.6384 - 1.035\delta_i + 3.7201\delta_i^2 - 5.1773\delta_i^3 + 7.553\delta_i^4 - 7.332\delta_i^5 + 2.4909\delta_i^6 \tag{7}$$

By equations (6) and (7), a crack extent (Δ_i) of values 0.03 and 0.05 correspond to crack depth of 33% and 41%, respectively, of the overall depth of the beam section *h*.

A characteristic equation is obtained by equations (3), (4), and (5). An infinite number of solutions can then be calculated and denoted by β_k for $k = 1, \ldots \infty$. For each β_k, the natural frequencies ω_k and mode shape ϕ_k of the system can be computed, and the overall response of the beam can be expressed as:

$$y(x,t) = \sum_{k=1}^{\infty} \phi_k(x)\, z_k(t) \tag{8}$$

where $\phi_k(x)$ is the mode shape function of the *k*th mode; $z_k(t)$ is the *k*th modal amplitude. By

assuming that all modes are uncoupled, and the damping ratio of the *k*th mode is ζ_k, the modal amplitude of the *k*th mode $z_k(t)$ can be calculated as:

$$\ddot{z}_k(t) + 2\zeta_k \omega_k \dot{z}_k(t) + \omega_k^2 z_k(t) = P_k(t) \tag{9}$$

where $P_k(t)$ is the excitation of the *k*th mode. The time-domain responses of the beam can then be calculated by the method of modal superposition.

According to Katafygiotis *et al.* (2000), the uncertainties associated with the stiffness of the rotational spring, which is employed to model the semi-rigid connection, are much larger than those associated with other model parameters, such as the modulus of elasticity and the mass density of the structural member. Therefore, it is proposed here that the rotational stiffnesses be included as uncertain parameters in the Bayesian statistical framework. It must be pointed out that an increase in uncertainties associated with the crack detection results is the tradeoff for including additional uncertain parameters without increasing the number of measured data points in *D*. The effects of including the rotational stiffnesses as uncertain parameters are illustrated in the numerical case study.

The numerical values of the rotational stiffnesses are of a different order of magnitude to other uncertain parameters, such as the damage locations and extents. In order to prevent a numerical problem, it is proposed here that the rotational stiffness be normalized by the bending rigidity of the beam as:

$$\tilde{K}_L = \frac{K_L}{EI} \quad and \quad \tilde{K}_R = \frac{K_R}{EI} \tag{10}$$

where $\tilde{K}_L$ and $\tilde{K}_R$ are the normalized rotational stiffnesses at the left and right ends of the beam respectively.

The reference system (healthy status) is represented by the model class M_0 ($j = 0$), in which the vector of uncertain model parameters is $\mathbf{a}_0 = \{\tilde{K}_L, \tilde{K}_R, \zeta\}^T$, where the subscript of $\mathbf{a}$ represents the number of cracks. Because the bending rigidity (EI) and the mass density (ρ) can usually be measured or calculated with a high degree of accuracy, they are not included as uncertain parameters in the numerical case study. In general, the uncertain parameter vector for the class of models with *j* cracks, M_j, is:

$$\mathbf{a}_j = \left\{\tilde{K}_L, \tilde{K}_R, \zeta, l_1, l_2, \ldots l_j, \Delta_1, \Delta_2, \ldots, \Delta_j\right\}^T \tag{11}$$

The total number of uncertain parameters is $2j + 3$. It is assumed that the damping ratios for all modes are the same and equal to ζ in order to reduce the number of uncertain parameters in

the Bayesian statistical framework.

2.2 Identification of the number of cracks by Bayesian model class selection

As shown in Figure 1, M_j is the class of models of beams with *j* crack for $j = 0,\ldots,N_M$, where M_0 corresponds to a beam with no crack; and N_M is the maximum number of cracks to be considered in the crack detection process. In the first phase of the proposed methodology, the goal is to use the set of measured dynamic data D to select the "best" class of models from among $N_M + 1$ prescribed classes of models. From equation (11), $\mathbf{a}_j \in S(\mathbf{a}_j) \subset R^{N_j}$ is the vector of uncertain model parameters, such as the crack locations and extents, to be identified following the Bayesian statistical framework, where N_j is the dimension of $\mathbf{a}_j$. By following the Bayes' theorem, the posterior (or updated) probability density function (PDF) $p(\mathbf{a}_j \mid D, M_j)$ for a given set of measurement *D* and model class M_j can be expressed as:

$$p(\mathbf{a}_j \mid D, M_j) = c_j\, p(\mathbf{a}_j \mid M_j)\, p(D \mid \mathbf{a}_j, M_j) \tag{12}$$

where c_j is a normalizing constant, and $p(\mathbf{a}_j \mid M_j) = \pi(\mathbf{a}_j)$ is the prior PDF of the set of uncertain model parameters $\mathbf{a}_j$, which allows the judgment about the relative plausibility of the values of the uncertain parameters to be incorporated. A uniform prior PDF, such that the posterior PDF depends solely on the data, can always be chosen; $p(D \mid \mathbf{a}_j, M_j)$ is the likelihood of the data given $\mathbf{a}_j$ of model class M_j, which, under the assumption of independent Gaussian prediction errors, is given by:

$$p(D \mid \mathbf{a}_j, M_j) = \frac{1}{\left(\sqrt{2\pi}\sigma_j\right)^{NN_O}} \exp\left[-\frac{NN_O}{2\sigma_j^2} J(\mathbf{a}_j \mid D, M_j)\right] \tag{13}$$

where σ_j is the standard deviation of the target error; *N* is the total number of measured data points at one observed degree of freedom (DOF); and N_O is the number of observed DOFs. The function $J(\mathbf{a}_j \mid D, M_j)$ in equation (13) is the contribution of the measured dynamic data, and is given by (Beck & Katafygiotis 1998):

$$J(\mathbf{a}_j \mid D, M_j) = \frac{1}{NN_O} \sum_{n=1}^{N} \left\| \hat{\mathbf{y}}(n) - \mathbf{q}_O(n; \mathbf{a}_j, M_j) \right\|^2 \tag{14}$$

where $\mathbf{q}_O(n; \mathbf{a}_j, M_j)$ is the vector of calculated response (at the observed DOFs) at the *n*th time step for a given model $\mathbf{a}_j$ in M_j; $\hat{\mathbf{y}}(n)$ is the vector of measured response, both

$\mathbf{q}_O\left(n;\mathbf{a}_j,M_j\right)$ and $\hat{\mathbf{y}}(n)$ are of dimensions N_o by 1; and $\|.\|$ denotes the Euclidean norm of a vector. A smaller value of $J\left(\mathbf{a}_j \mid D,M_j\right)$ in equation (14) implies a better fit to the measurement by the corresponding model $\mathbf{a}_j$. The "optimal" (or "best") model $\mathbf{a}_j$ in a given model class M_j for a given set of data *D* can be identified by maximizing the posterior PDF $p\left(\mathbf{a}_j \mid D,M_j\right)$ in equation (12). When a uniform prior PDF (non-informative prior) is chosen in equation (12), this is equivalent to maximizing the likelihood $p\left(D \mid \mathbf{a}_j,M_j\right)$ in equation (13) or minimizing the $J\left(\mathbf{a}_j \mid D,M_j\right)$ function in equation (14).

According to Cox (1961), probability can be interpreted as a measure of plausibility based on specified information. In other words, the probability of a class of models conditional on the set of dynamic data *D* is required in order to determine the most plausible model class. This conditional probability can be formulated by again following the Bayes' theorem as (Beck & Yuen 2004):

$$P\left(M_j \mid D,U\right)=\frac{p\left(D \mid M_j,U\right)P\left(M_j \mid U\right)}{p\left(D \mid U\right)} \quad \text{for} \quad j=0,...,N_M \tag{15}$$

where $p(D \mid U)=\sum_{j=0}^{N_M} p\left(D \mid M_j,U\right)p\left(M_j \mid U\right)$ by the theorem of total probability (Beck & Yuen 2004), and $1/p(D \mid U)$ can be treated as a normalizing constant; U expresses the user's judgment on the initial plausibility of the model classes; $P\left(M_j \mid U\right)$ is the prior probability of the model class M_j based on the judgment of engineers, where $\sum_{j=0}^{N_M} P\left(M_j \mid U\right)=1$. Unless there is prior information about the number of cracks on the beam, the prior probability $P(M_j \mid U)$ can be taken as $1/(N_M+1)$. The most important term in equation (15) is the evidence $p(D \mid M_j,U)$ for the model class M_j provided by the data *D*. The class of models to be used is obviously the one that maximizes the probability $P(M_j \mid D,U)$ and this is in general equivalent to the one that maximizes the evidence $p(D \mid M_j,U)$ with respect to M_j. It must be pointed out that U is irrelevant in $p(D \mid M_j,U)$ and so it can be dropped hereafter in the notations because it is assumed that M_j alone specifies the PDF for the data.

For a globally identifiable case, the evidence can be calculated based on an asymptotic approximation (Papadimitriou *et al.* 1997):

$$p\left(D \mid M_j\right) \approx p\left(D \mid \hat{\mathbf{a}}_j,M_j\right)(2\pi)^{\frac{N_j}{2}}\, p\left(\hat{\mathbf{a}}_j \mid M_j\right)\left|\mathbf{H}_j\left(\hat{\mathbf{a}}_j\right)\right|^{-\frac{1}{2}} \quad \text{for} \quad j=0,\ldots,N_M \tag{16}$$

where $\hat{\mathbf{a}}_j$ denotes the optimal model in the model class M_j (the set of optimal model parameters $\mathbf{a}_j$). $\hat{\mathbf{a}}_j$ can be obtained by maximizing the posterior PDF $p(\mathbf{a}_j \mid D, M_j)$ in equation (12); N_j is the number of uncertain model parameters in $\hat{\mathbf{a}}_j$; $\mathbf{H}_j(\hat{\mathbf{a}}_j)$ is the Hessian of the function $g(\mathbf{a}_j)$ evaluated at the optimal model $\hat{\mathbf{a}}_j$, where $g(\mathbf{a}_j)$ is given by:

$$g(\mathbf{a}_j) = -\ln\left[p(\mathbf{a}_j \mid M_j)p(D \mid \mathbf{a}_j, M_j)\right] \tag{17}$$

For unidentifiable cases, the evidence $p(D \mid M_j)$ can be calculated by using an extension of the asymptotic expansion used in equation (16) (Beck and Katafygiotis 1998; Katafygiotis *et al.* 1998). The discussion here will focus on globally identifiable cases. The interested reader is directed to references (Beck and Katafygiotis 1998; Katafygiotis *et al.* 1998; Katafygiotis *et al.* 2000) and (Katafygiotis *et al.* 2000; Katafygiotis and Lam 2002) for, respectively, details about the classification of identifiable and unidentifiable problems and the approximation of the likelihood $p(D \mid \mathbf{a}_j, M_j)$ in equation (12) in the general unidentifiable problem.

The evidence $p(D \mid M_j)$ in equation (16) consists of two factors. The first factor $p(D \mid \hat{\mathbf{a}}_j, M_j)$ is the likelihood factor. This will be larger for those model classes that make the probability of the data *D* higher, that is, those that give a better "fit" to the data, which favors model classes with more parameters (model classes with higher complexity). The second factor $(2\pi)^{N_j/2}\, p(\hat{\mathbf{a}}_j \mid M_j)\,|\mathbf{H}_j(\hat{\mathbf{a}}_j)|^{-1/2}$ is called the Ockham factor (Gull 1988). Beck and Yuen (2004) showed that the value of the Ockham factor decreases as the number of uncertain parameters in the model class increases and, therefore, it provides a mathematically rigorous and robust penalty against parameterization. The combination of these two factors allows to select a model class that, on one hand, is complex enough to provide a "good fit" to the measurement but, on the other hand, is not so complex that it "over fits" the data.

The proposed algorithm for identifying the number of cracks on the beam is summarized as follows:

1. Initialize the index $j = 0$, and calculate the evidence $p(D \mid M_j)$ for the beam without crack by equation (16).
2. Increase the index *j* by 1 ($j = j + 1$), and calculate the evidence $p(D \mid M_j)$ for the beam with single crack.
3. Compare the evidence of $p(D \mid M_{j-1})$ with that of $p(D \mid M_j)$. If $p(D \mid M_{j-1}) > p(D \mid M_j)$, then M_{j-1} is the "best" class of models. Otherwise, increase the

index j by 1 ($j = j + 1$) and repeat this step.

By following this simple algorithm, the proposed methodology can identify the number of cracks, say N_C, by calculating the evidence of the model classes M_0, M_1, …, M_{N_C+1}. The maximum number of cracks to be considered N_M is equal to $N_C + 1$. It should be noted that during the calculation of the evidence $p(D|M_j)$, the uncertain model parameters are determined by optimizing equation (13).

2.3 Identification of the updated PDF of crack locations and extents by Bayesian statistical framework

After identifying the number of cracks N_C, by the Bayesian model class selection method, the goal in the second phase is to calculate the posterior PDF $p\left(\mathbf{a}_{N_C} | D, M_{N_C}\right)$ of the set of uncertain model parameters $\mathbf{a}_{N_C}$ in the model class M_{N_C}. This can be obtained from equation (12) by setting $j = N_C$.

For a globally identifiable case, Beck and Katafygiotis (1998) demonstrated that the posterior PDF $p\left(\mathbf{a}_{N_C} | D, M_{N_C}\right)$ is very peaked at a finite number of optimal models that globally minimize the $J\left(\mathbf{a}_{N_C} | D, M_{N_C}\right)$ function in equation (14) (with $j = N_C$) within the bounded parameter space $S\left(\mathbf{a}_{N_C}\right)$. By following the algorithm presented in Katafygiotis & Beck (1998), the finite set of optimal models $\hat{\mathbf{a}}_{N_C}^{(q)}$ for $q = 1, \ldots, N_q$ can be identified, where N_q is the total number of global optimal models in $S\left(\mathbf{a}_{N_C}\right)$.

The posterior PDF of the model parameters $\mathbf{a}_{N_C}$ for the given set of dynamic measurement D and model class M_{N_C} can then be approximated as a weighted sum of Gaussian distributions centered at the N_q optimal models, as in Beck and Katafygiotis (1998):

$$p\left(\mathbf{a}_{N_C} | D, M_{N_C}\right) \approx \sum_{q=1}^{N_q} w_q \mathbf{N}\left(\hat{\mathbf{a}}_{N_C}^{(q)}, A_N^{-1}\left(\hat{\mathbf{a}}_{N_C}^{(q)}\right)\right) \tag{18}$$

where $\mathbf{N}(\boldsymbol{\mu}, \boldsymbol{\Sigma})$ denotes a multivariate Gaussian distribution with mean $\boldsymbol{\mu}$ and covariance matrix $\boldsymbol{\Sigma}$. The covariance matrix $A_N^{-1}\left(\hat{\mathbf{a}}_{N_C}^{(q)}\right)$ is the Hessian of the function $N_J \ln J\left(\mathbf{a}_{N_C} | D, M_{N_C}\right)$ evaluated at $\hat{\mathbf{a}}_{N_C}^{(q)}$, where $J\left(\mathbf{a}_{N_C} | D, M_{N_C}\right)$ is given by equation (14) and $N_J = (NN_o - 1)/2$. The weighting coefficients in equation (18) are given by:

$$w_q = \frac{w'_q}{\sum_{q=1}^{N_q} w'_q} \quad \text{where} \quad w'_q = \pi\left(\hat{\mathbf{a}}_{N_C}^{(q)}\right)\left|A_N\left(\hat{\mathbf{a}}_{N_C}^{(q)}\right)\right|^{-\frac{1}{2}} \tag{19}$$

where $\pi\left(\hat{\mathbf{a}}_{N_C}^{(q)}\right)$ is the prior PDF $p\left(\mathbf{a}_{N_C} | M_{N_C}\right)$ in equation (12) of the set of uncertain model parameters $\mathbf{a}_{N_C}$ evaluated at $\hat{\mathbf{a}}_{N_C}^{(q)}$.

Instead of pinpointing the crack locations and extents, the proposed crack detection methodology focuses on calculating the posterior PDF of the model parameters $\mathbf{a}_{N_C}$. As a result, the level of the crack detection results can be quantified with confidence. This information is extremely important for engineers who are making judgments about remedial work.

3 Numerical Case Study

A Bernoulli-Euler beam with length 0.4 m is employed in the numerical case study presented here to verify the proposed crack detection methodology. Because there is no perfectly rigid or pin connection in a real situation, the beam end connections are considered to be semi-rigid and are modeled by rotational springs with constant stiffnesses. The nominal dimensions and material properties of the beam are summarized in Table 1. In the simulation of measured dynamic responses, the beam is assumed to be classically damped with a critical damping ratio of 1% for all modes ($\zeta = 0.01$). Measurement noise is considered by adding a 5% white noise to the calculated dynamic responses in all cases. Only 0.4 sec of data with 1000 Hz sampling frequency is employed in the crack detection process and, therefore, the number of measured data points *N* in equation (13) is 401. Four sensors are evenly installed on the beam for measuring the vertical vibration at 0.08 m, 0.16 m, 0.24 m, and 0.32 m from the left end of the beam.

The results of six cases (Cases A to F) are presented in this paper. The case identification, true values of crack number, rotational stiffness, and crack parameters, together with the vector of uncertain parameters of the class of identification model for all cases, are summarized in Table 2. In the last column of the table, the index *j* represents the number of cracks considered in the class of identification models. Note that there is no l_j or Δ_j in the list of uncertain parameters for M_0 (the model class of undamaged beam). For Cases A and C, they are $\mathbf{a}_j = \left\{\tilde{K}_L, \tilde{K}_R, \zeta\right\}$ and $\mathbf{a}_j = \left\{\tilde{K}, \zeta\right\}$, respectively.

In Cases A, B, and C, there is only one crack at 0.18 m from the left end of the beam ($l_1 = 0.18$ m) with crack extent $\Delta_1 = 0.05$ (the depth of the crack is 41% of the beam depth). The normalized rotational stiffnesses at the left and right ends of the beam are 0.1 and 0.2, respectively. Furthermore, the impact force is applied at the middle of the beam. Case A is used to illustrate the proposed crack detection methodology procedure. The main purpose of Cases B and C is to test the effects of model complexity and model error on the results of crack detection.

In Case D, there are two cracks at 0.14 m and 0.18 m from the left end of the beam ($l_1 = 0.14$ m and $l_2 = 0.04$ m measured from the location of the first crack) with crack extents $\Delta_1 = 0.05$ and $\Delta_2 = 0.03$, respectively (the depth of the crack is about 40% and 32%, respectively, of the beam depth). The purpose of Case D is to verify the use of the proposed methodology in situations in which there is more than one crack on the beam. Case E also has two cracks, but the crack extents are smaller than those in Case D ($\Delta_1 = \Delta_2 = 0.01$, equivalent to a crack depth of 19% of the beam depth). There are three cracks in Case F, which are at 0.14 m, 0.18 m, and 0.26 m from the left end of the beam ($l_1 = 0.14$ m, $l_2 = 0.04$ m, and $l_3 = 0.08$ m) with crack extents equal to 0.05, 0.03, and 0.04, respectively ($\Delta_1 = 0.05$, $\Delta_2 = 0.03$, and $\Delta_3 = 0.04$). These final two cases are used to test the proposed methodology in small crack and multi-crack situations. For Cases D, E, and F, the rotational stiffnesses of the left and right ends of the beam are 0.2 and 0.4, respectively, and the impact location is at one third of the beam.

3.1 Case A

Case A is a simple case to demonstrate the procedures of the proposed methodology when there are only one crack on the beam. In this case, the left and right normalized rotational stiffnesses ($\tilde{K}_L$ and $\tilde{K}_R$), together with the damping ratio (ζ), are considered as uncertain parameters in the class of identification models.

The proposed crack detection methodology begins by calculating the logarithm of the evidence in equation (16) for M_0 and M_1, which are the model classes for beams with zero and single crack, respectively. The logarithm is used because the numerical values of the evidence are usually very large, which may cause computational problems. The calculated results are summarized in Table 3. It is clear from the table that the logarithm of the evidence of

M_1 (12837) is larger than that of M_0 (8282) and, therefore, it can be concluded that the beam is cracked and the undamaged hypothesis can be ruled out. The evidence of the class of models M_2 (beams with two cracks) is then calculated and summarized in Table 3. As the logarithm of the evidence of M_2 (12831) is smaller than that of M_1 (12837), it is concluded that there is only one crack on the beam, and it is not necessary to test other classes of models corresponding to three or more cracks. The proposed methodology successfully identifies the true number of cracks ($N_C = 1$) in this case. Table 3 also shows the logarithms of the likelihood and Ockham factors of the evidence. As discussed in Section 2.2, the likelihood factor is increasing and the Ockham factor is decreasing (i.e., its logarithm becomes more negative) as the model class becomes more complex (i.e., there are more model parameters). It must be pointed out that if a class of models is selected based solely on the ability of the model class to fit the measurement (i.e., the likelihood factor alone), the most complex model class will always be chosen.

Based on the proposed crack detection method, the optimal model $\hat{\mathbf{a}}_1$ and the updated PDF of the set of model parameters $\mathbf{a}_1$ can be calculated. The normalized marginal PDF of the crack location and extent for the crack (l_1 vs. Δ_1) are plotted in Figure 3. Because there is only one optimal model within the domain of interest, there is only one peak in the marginal PDF plot. The figures also show that the PDF value drops significantly when one moves away from the optimal model $\hat{\mathbf{a}}_1$ in any direction. This is the typical characteristic of an identifiable case (Katafygiotis & Lam 2002) in model updating or structural health monitoring. The marginal cumulative distributions of all crack parameters are then calculated and plotted in Figures 4 and 5. These figures provide detailed information about the uncertainties associated with the two crack parameters. For purpose of discussion, the coefficients of variation (COVs) for all uncertain parameters are calculated based on the updated PDFs and summarized together with the optimal parameters in Table 9. From the first row of the table (Case A), the identified crack location and extent are 0.1797 m and 0.0520 m, respectively. These are very close to the true values. The identified normalized rotational stiffnesses of the left and right ends of the beam are 0.0981 and 0.2449, respectively. Although the identified value of the rotational stiffness of the right spring is not as accurate as that for other parameters, this can be explained by the relatively large COV (26.65%). The results show that the uncertainties associated with the rotational stiffnesses are much higher than those of other parameters. This result is consistent with the findings of Katafygiotis *et al.* (2000). The identified damping is close to the true value and the corresponding COV is small. The low uncertainty of the damping ratio is due to the fact that

both the simulated and the modeled dynamic responses are assumed to be classically damped. In the absence of model error in damping, the low uncertainty in the identified damping ratio is expected.

3.2 Case B

As mentioned in Section 2.1, the number of uncertain parameters has a significant effect on the uncertainties associated with the identification results. In order to demonstrate this effect, Case B assumes that the rotational stiffnesses of the left and right rotational springs together with the damping ratio are given. Although the exact values of these parameters would be impossible to obtain in a real situation, a comparison between Cases A and B helps in an understanding of the effect and importance of model class complexity on the result of crack detection (or system identification).

Because there are no uncertain parameters in M_0, it is meaningless to calculate the evidence of this model class. If there is no crack on the beam, the calculated responses from the model in M_0 must be very similar to those from the measurement. Figure 6 shows the measured response and the calculated response by the model in M_0. Because the responses are very different, it is impossible for M_0 to be the true class of models, and it can therefore be concluded that there must be "some cracks" on the beam. In order to identify the number of cracks, the logarithms of the evidence for the model classes M_1 and M_2 are calculated and summarized in Table 4. It is clear from the table that M_1 is the most probable class of models and, therefore, it can be concluded that there is only one crack on the beam.

The optimal parameters, together with the updated PDF, can then be calculated. The marginal cumulative distributions of the crack location and extent are plotted in Figures 7 and 8, respectively. Note that Figures 7 and 4 are plotted in the same scale and, therefore, they can be directly compared. By comparing these two figures, it becomes clear that the uncertainty of the identified crack location in Case A is much higher than that in Case B. A very similar conclusion can be drawn from comparing Figures 5 and 8 for the uncertainties associated with the identified crack extents in Cases A and B. The COVs are then calculated and summarized in the brackets of Table 9. As expected, the identified crack location and extent are close to their true values. A comparison of the COVs in Cases A and B shows that the uncertainties of the identified crack parameters in Case A are much higher than those in Case B, as suggested by the marginal cumulative distributions in Figures 4, 5, 7, and 8. Because the only difference between

Cases A and B is the number of uncertain parameters, the reduction in uncertainties from Case A to Case B must be caused by the decrease in model complexity.

When the evidence of M_1 in Case A (12837 in Table 3) is compared with that in Case B (12850 in Table 4), it can be concluded that the M_1 model class in Case B is "better" than that in Case A. This is obvious, because the exact values of rotational stiffnesses and damping ratio are employed in Case B.

3.3 Case C

Case C is the same as Case A except that the two rotational springs in Case C are assumed to be the same and are parameterized by a parameter $\tilde{K}$ in the class of identification models. This arrangement, on the one hand, reduces the number of uncertain parameters, but, on the other hand, introduces model error because the rotational stiffnesses of the real structure are different at the two ends.

The evidence for the classes of models M_0 (8348), M_1 (12838), and M_2 (12833) are calculated and shown in Table 5. The proposed methodology selects M_1 to be the "best" model class, and this is the correct answer. The identified optimal parameters and the corresponding COVs are summarized in the third row of Table 9. As the PDFs are similar to those in the previous cases, they are not shown. Once again, the identified crack parameters are very close to the true values. Note that the identified normalized rotational stiffness is 0.1884, which is in between the simulated values at the left (0.1) and right (0.2) ends of the beam.

The COVs for crack location and extent in Case C are close to those in Case A, but much larger than those in Case B. On one hand, the reduction in model complexity from Case A to Case C reduces the uncertainties associated with the identification result, but, on the other hand, the introduced model error increases those uncertainties. As a result, the uncertainties of the identification results for Cases A and C are very similar.

The study of Cases A to C shows also the effect of model complexity in the required computational cost. Firstly, the computational time required for calculating the time-domain responses of a more complex model class is longer. Secondly, a model class with more uncertain parameters will result in a larger number of minimization variables in the minimization of the *J* function in equation (14). This in terms will lead to a larger number of iteration steps in the numerical optimization process, and therefore, a longer computational time. However, the computational time required for analyzing a beam is very short even in Case

A (the most complex model class among the three cases).

When the evidence of M_1 in Case A (12837 in Table 3) is compared with that in Case C (12838 in Table 5), it is clear that M_1 in Case C is slightly "better" than that in Case A. However, the difference between the logarithms of the evidence in the two cases is so small that the two model classes can be considered of similar quality each other.

3.4 Case D

This case is used to test the proposed methodology in a situation in which there is more than one crack on the beam. The proposed crack detection methodology starts by calculating the logarithm of the evidence in equation (16) for M_0 and M_1. From Table 6, it is clear that the logarithm of the evidence of M_1 (12996) is larger than that of M_0 (8389) and, therefore, it can be concluded that the beam is cracked. The evidence of the class of models M_2 (beams with two cracks) is then calculated and is equal to 13001 (see Table 6). As the logarithm of the evidence of M_2 is larger than that of M_1, it is concluded that there is more than one crack on the beam. The algorithm continues to calculate the logarithm of the evidence of M_3, which is equal to 12995 and is smaller than that of M_2. Therefore, it can be concluded that there are only two cracks on the beam. The proposed methodology successfully identifies the true number of cracks ($N_C = 2$) in this case. The fourth row of Table 9 (Case D) shows that the identified locations of the first and second cracks are 0.1412 m and 0.0349 m, respectively. These are close to the true values (0.14 m and 0.04 m). The identified extents of the first and second cracks are 0.0490 and 0.0283, respectively, which are again very close to the true values (0.05 and 0.03). The proposed methodology successfully identifies the crack parameters in this case.

3.5 Case E

Case E tests the proposed methodology in situations in which the crack extent is small (18% of the overall depth of the beam). Table 7 shows the logarithms of the evidence of M_0 (12935), M_1 (13135), M_2 (13149), and M_3 (13144) in Case E. It is clear from the table that there are only two cracks on the beam. The optimal parameters and the corresponding COVs are calculated and summarized in the fifth row of Table 9. The identified crack location and extent are again very close to the true values. The proposed crack detection methodology has no

problem in identifying the simulated cracks even when the crack depths are small. When the COVs of the identified parameters in Case E are compared with those in Case D, it appears that the uncertainties associated with the crack parameters are relatively higher when the crack extent is small.

3.6 Case F

Unlike all of the previous cases, Case F presents a situation in which there are three cracks with different crack depths. The logarithms of the evidence of the classes of models with zero to four cracks are calculated and summarized in Table 8. The logarithm of evidence increases from M_0 to M_3 (from 8303 to 12956) and decreases from M_3 to M_4 (from 12956 to 12948), demonstrating that the correct number of cracks is three. The last row of Table 9 shows that the identified crack locations and the corresponding extents are very close to the true values as shown in Table 2. Therefore, it can be concluded that the proposed methodology successfully identifies the damage in this case.

4 Concluding Remarks

This paper addresses the problem of crack detection in beams utilizing a set of measured dynamic data. Unlike other crack detection methods in the literature, the proposed methodology is applicable to multi-crack cases even when the number of cracks is not known in advance. The proposed methodology relies on the Bayesian model class selection method to identify the number of cracks based on the set of dynamic measurements. The updated PDF of the crack location, extent, and other uncertain model parameters, such as the rotational stiffness for modeling the semi-rigid behavior of the beam end connections and the damping ratio, is calculated by the Bayesian statistical framework.

A Bernoulli-Euler beam with semi-rigid connections at both ends is employed to verify the proposed methodology in a numerical case study. The results show that the proposed crack detection methodology can successfully identify the simulated cracks in the presence of measurement noise and/or modeling error. It must be pointed out that the effect of modeling error may increase when field test data is used instead of computer simulated data. Under such situation the Timoshenko beam model can be employed as the model classes of cracked beams in order to reduce the effect of modeling error in the results of crack detection.

The effects of the complexity of model class on the uncertainties of the crack detection

results are also considered in the case study. In the absence of model error, the higher the model complexity (more model parameters), the higher the uncertainties associated with the identification results will be. When there is model error, the increase in model complexity may help in reducing it, and thus decreasing the uncertainties in the results of crack detection. Although the overall effect differs from case to case, the Bayesian statistical framework provides a robust measure to quantify this uncertainty.

5 Acknowledgements

The work described in this paper was fully supported by a grant from the Research Grants Council of the Hong Kong Special Administrative Region, China (Project No. CityU 1190/04E).

6 References

[1] Beck, J.L. and Katafygiotis, L.S. 1998. Updating models and their uncertainties I: Bayesian statistical framework, Journal of Engineering Mechanics, ASCE, 124(4), pp. 455-461.

[2] Beck, J.L. and Yuen, K.V. 2004. Model selection using response measurement: A Bayesian probabilistic approach, Journal of Engineering Mechanics, ASCE, 130(2), pp. 192-203.

[3] Cawley, P. and Adams, R.D. 1979. The location of defects in structures from measurements of natural frequencies, Journal of Strain Analysis, 14(2), pp. 49-57.

[4] Chen, W.F. and Kishi, N. 1989. Semirigid steel beam-to-column connections: data base and modeling, Journal of Structural Engineering, 116(1), pp. 105-119.

[5] Cox, R.T. 1961. The algebra of probable inference, The Johns Hopkins University Press, Baltimore.

[6] Gull, S.F. 1988. Bayesian inductive inference and maximum entropy, maximum entropy and Bayesian methods (Ed. J. Skilling), Kluwer Academic Publisher, Boston, pp. 53-74.

[7] Katafygiotis, L.S. and Beck, J.L. 1998. Updating models and their uncertainties II: model identifiability, Journal of Engineering Mechanics, ASCE, 124(4), pp. 463-467.

[8] Katafygiotis, L.S. and Lam, H.F. 2002. Tangential-projection algorithm for manifold

representation in unidentifiable model updating problems, Earthquake Engineering & Structural Dynamics, 31 (4), pp. 791-812.

[9] Katafygiotis, L.S., Lam, H.F., and Papadimitriou, C. 2000. Treatment of unidentifiability in structural model updating, Advances in Structural Engineering, 3(1), pp. 19-39.

[10] Katafygiotis, L.S., Papadimitriou, C., and Lam, H.F. 1998. A probabilistic approach to structural model updating, Soil Dynamics and Earthquake Engineering, 17(7-8), pp. 495-507.

[11] Lam, H.F., Lee, Y.Y., Sun, H.Y., Cheng, G.F., and Guo, X. 2005. Application of the spatial wavelet transform and Bayesian approach to the crack detection of a partially obstructed beam, Thin-Walled Structures, 43, pp. 1-12.

[12] Law, S.S. and Lu, Z.R. 2005. Crack identification in beam from dynamic responses, Journal of Sound and Vibration, 285(4-5), pp. 967-987.

[13] Liang, R.Y., Choy, F.K., and Hu, J. 1991. Detection of cracks in beam structures using measurements of natural frequencies, Journal of the Franklin Institute, 328(4), pp. 505-518.

[14] Nandwana, B.P. and Maiti, S.K. 1997. Modeling of vibration of beam in presence of inclined edge or internal crack for its possible detection based on frequency measurements, Engineering Fracture Mechanics, 58(3), pp. 193-205.

[15] Narkis, Y. 1994. Identification of crack location in vibrating simply supported beams, Journal of Sound and Vibration, 172(4), pp. 549-558.

[16] Ostachowicz, W.M. and Krawczuk, M. 1991. Analysis of the effect of cracks on the natural frequencies of a cantilever beam, Journal of Sound and Vibration, 150(2), pp. 191-201.

[17] Papadimitriou, C., Beck, J.L., and Katafygiotis, L.S. 1997. Asymptotic expansions for reliability and moments of uncertain systems, Journal of Engineering Mechanics, ASCE, 123(12), pp. 1219-1229.

[18] Rizos P.F., Aspragathos N., and Dimarogonas, A.D. 1990. Identification of crack location and magnitude in a cantilever beam from the vibration modes, Journal of Sound and Vibration, 138(3), pp. 381-388.

[19] Ruotolo, R. and Surace, C. 1997. Damage assessment of multiple cracked beams: Numerical results and experimental validation, Journal of Sound and Vibration, 206(4), pp. 567-588.

[20] Sohn, H., Farrar, C.R., Hernez, F.M., Czarnecki, J.J., Shunk, D.D., Stinemates, D.W.,

and Nadler, B.R. 2004. A review of structural health monitoring literature: 1996 – 2001, Los Alamos National Laboratory Report, LA-13976-MS.

Figure List

Figure 1: Schematic diagram illustrating the basic strategy for identifying the number of cracks 23

Figure 2: The model of a cracked beam with semi-rigid connections at both ends 24

Figure 3: Normalized marginal PDF of the crack location (l_1) and extent (Δ_1) in Case A . 25

Figure 4: Marginal cumulative distribution of the crack location (l_1) in Case A..... 26

Figure 5: Marginal cumulative distribution of the crack extent (Δ_1) in Case A 27

Figure 6: Measured response vs. calculated response of the model in M_0 in Case B (sensor at 0.16 m from the left end of the beam) 28

Figure 7 : Marginal cumulative distribution of the crack location (l_1) in Case B..... 29

Figure 8: Marginal cumulative distribution of the crack extent (Δ_1) in Case B 30

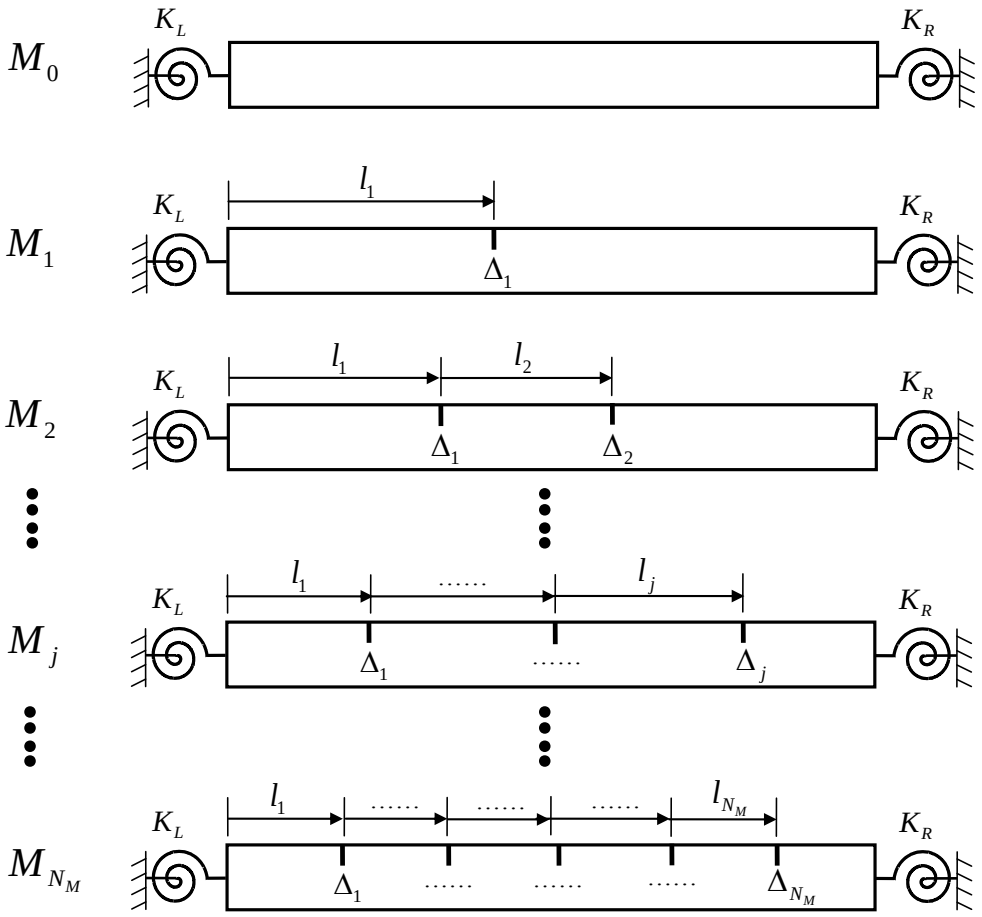

Figure 1: Schematic diagram illustrating the basic strategy for identifying the number of cracks

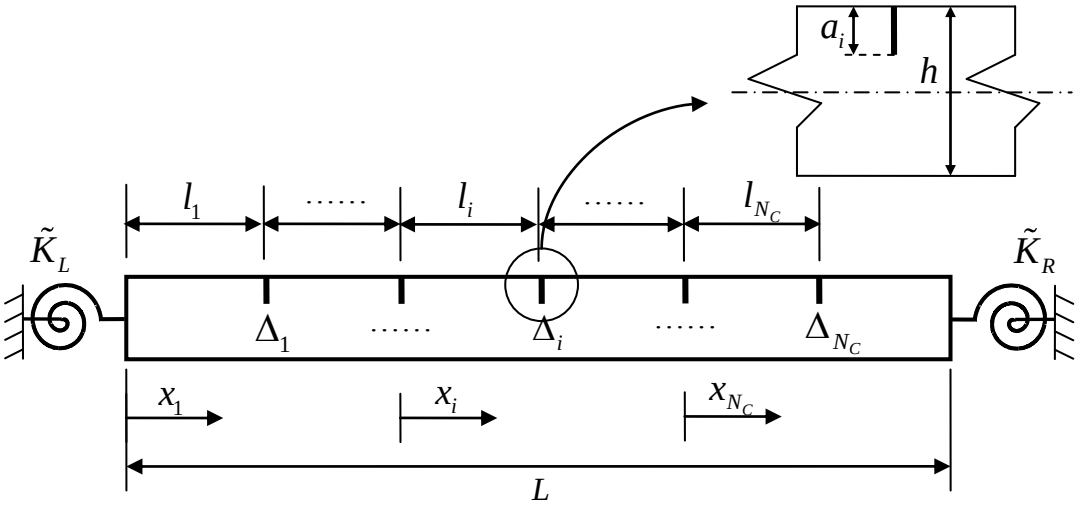

Figure 2: The model of a cracked beam with semi-rigid connections at both ends

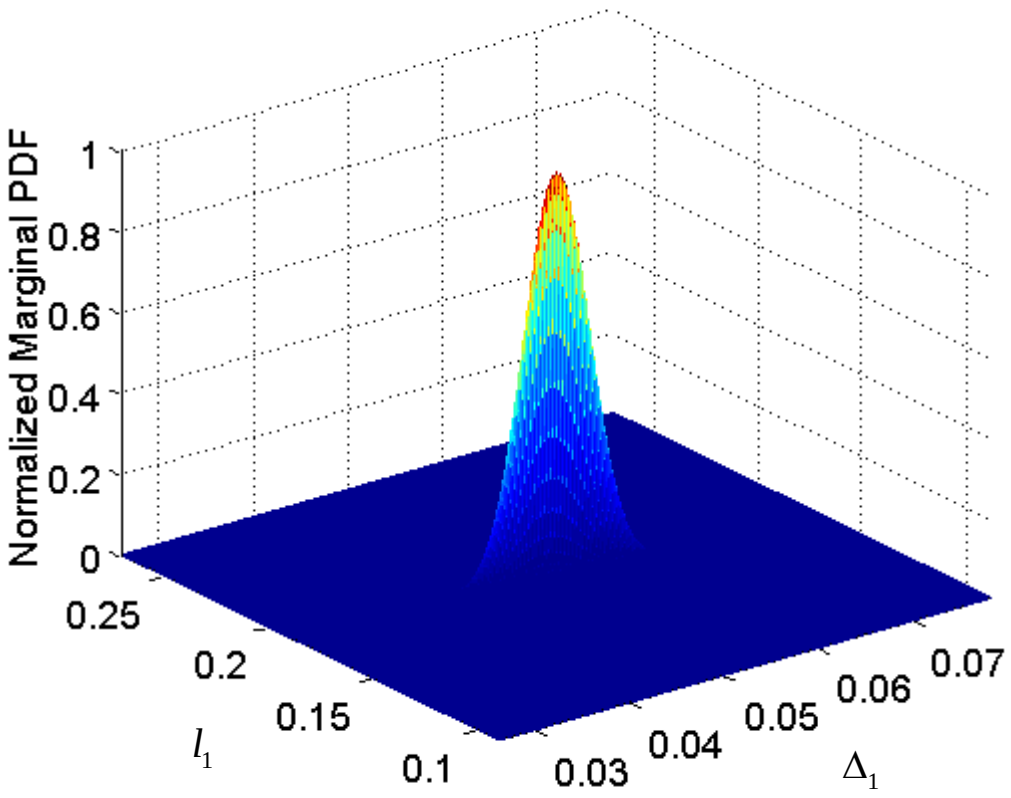

Figure 3: Normalized marginal PDF of the crack location (l_1) and extent (Δ_1) in Case A

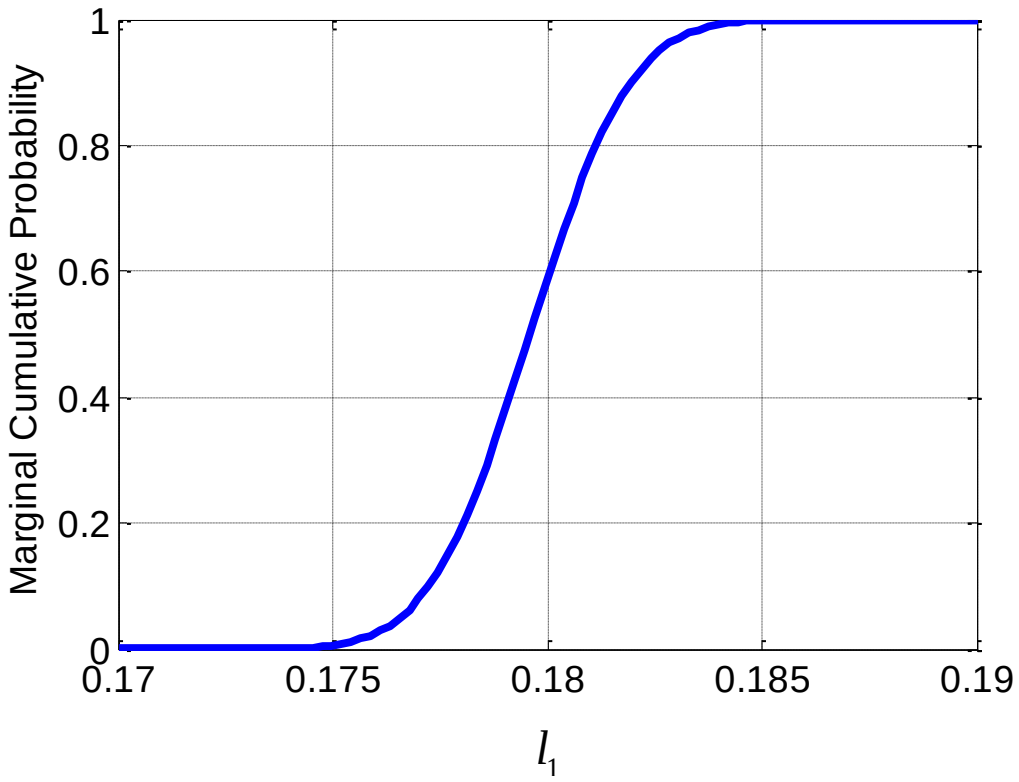

Figure 4: Marginal cumulative distribution of the crack location (l_1) in Case A

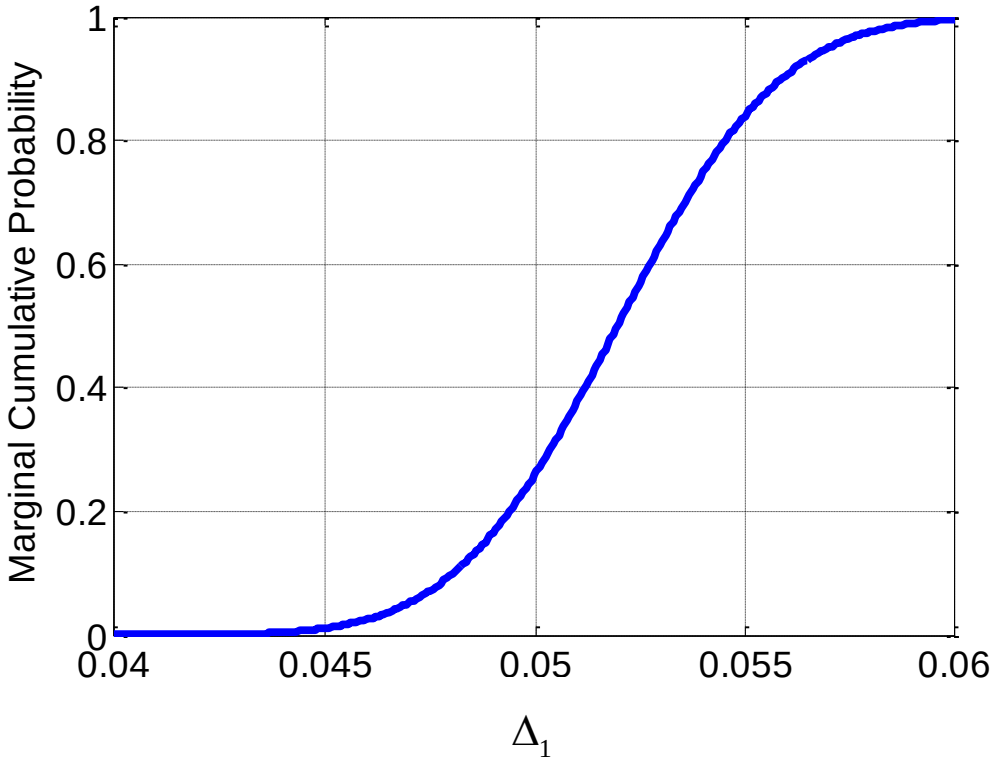

Figure 5: Marginal cumulative distribution of the crack extent (Δ_1) in Case A

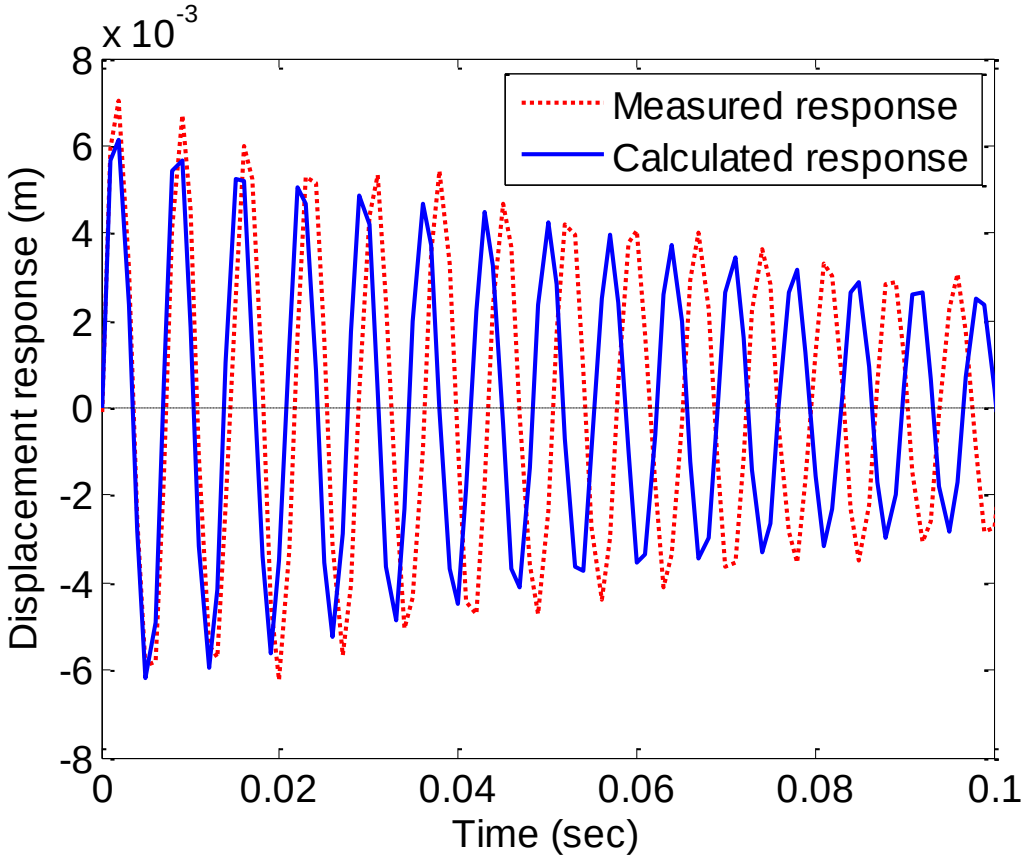

Figure 6: Measured response vs. calculated response of the model in M_0 in Case B (sensor at 0.16 m from the left end of the beam)

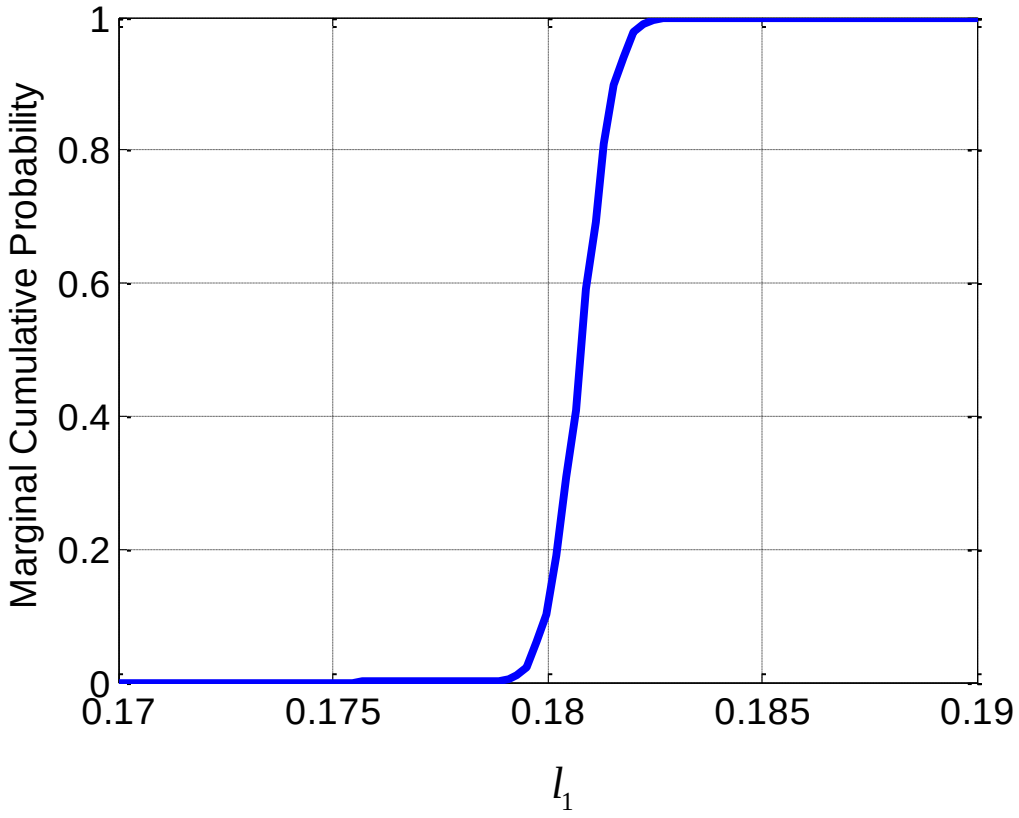

Figure 7 : Marginal cumulative distribution of the crack location (l_1) in Case B

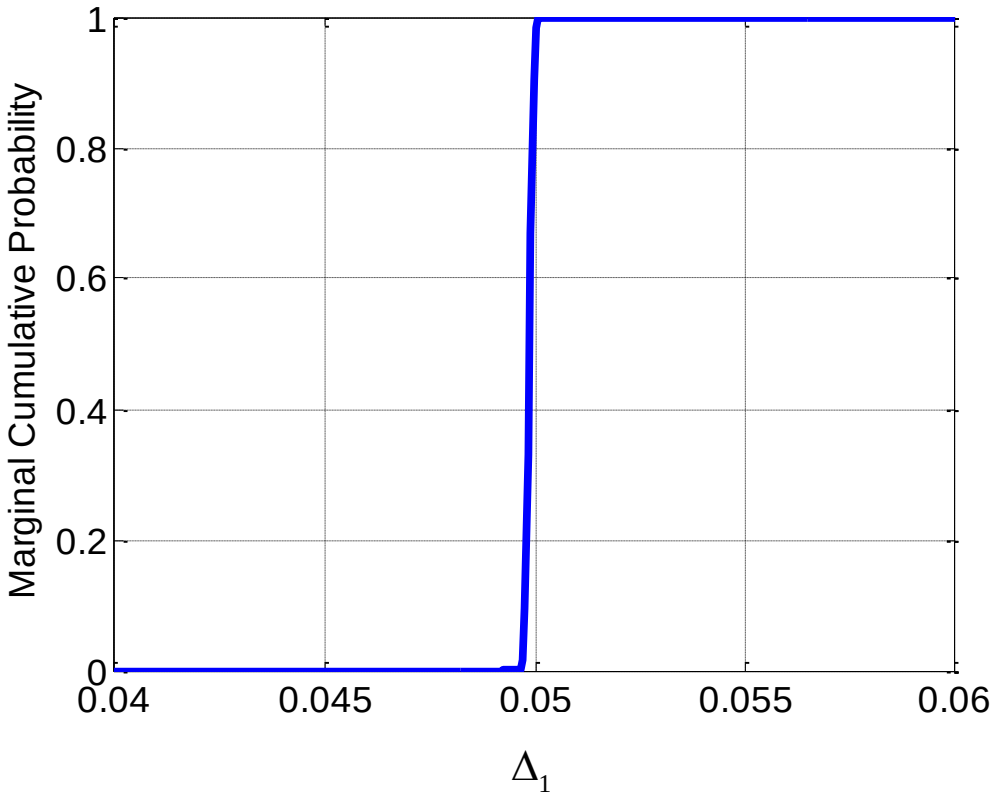

Figure 8: Marginal cumulative distribution of the crack extent (Δ_1) in Case B

Table List

Table 1: Member properties of the beam used in the numerical case study 32
Table 2: Summary of all cases in the numerical case study 33
Table 3: Evidence of different classes of models in Case A 34
Table 4: Evidence of different classes of models in Case B 35
Table 5: Evidence of different classes of models in Case C 36
Table 6: Evidence of different classes of models in Case D 37
Table 7: Evidence of different classes of models in Case E 38
Table 8: Evidence of different classes of models in Case F 39
Table 9: Optimal parameters and the corresponding COV in all cases 40

Property	Value
Length (L)	0.4 m
Depth of beam (h)	0.01 m
Width of beam (b)	0.01 m
Young's modulus (E)	200 GPa
Mass per unit length (m)	0.79 kg/m

Table 1: Member properties of the beam used in the numerical case study

Case	N_C	$(\tilde{K}_L, \tilde{K}_R)$	Crack Information	Uncertain parameters of the class of identification model M_j
A	1	(0.1, 0.2)	$l_1 = 0.18,\ \Delta_1 = 0.05$	$\mathbf{a}_j = \{\tilde{K}_L, \tilde{K}_R, \zeta, l_1, \ldots, l_j, \Delta_1, \ldots \Delta_j\}$
B	1	(0.1, 0.2)	$l_1 = 0.18,\ \Delta_1 = 0.05$	$\mathbf{a}_j = \{l_1, \ldots, l_j, \Delta_1, \ldots \Delta_j\}$
C	1	(0.1, 0.2)	$l_1 = 0.18,\ \Delta_1 = 0.05$	$\mathbf{a}_j = \{\tilde{K}, \zeta, l_1, \ldots, l_j, \Delta_1, \ldots \Delta_j\}$
D	2	(0.2, 0.4)	$l_1 = 0.14,\ \Delta_1 = 0.05$ $l_2 = 0.04,\ \Delta_2 = 0.03$	$\mathbf{a}_j = \{\tilde{K}_L, \tilde{K}_R, \zeta, l_1, \ldots, l_j, \Delta_1, \ldots \Delta_j\}$
E	2	(0.2, 0.4)	$l_1 = 0.14,\ \Delta_1 = 0.01$ $l_2 = 0.04,\ \Delta_2 = 0.01$	$\mathbf{a}_j = \{\tilde{K}_L, \tilde{K}_R, \zeta, l_1, \ldots, l_j, \Delta_1, \ldots \Delta_j\}$
F	3	(0.2, 0.4)	$l_1 = 0.14,\ \Delta_1 = 0.05$ $l_2 = 0.04,\ \Delta_2 = 0.03$ $l_3 = 0.08,\ \Delta_3 = 0.04$	$\mathbf{a}_j = \{\tilde{K}_L, \tilde{K}_R, \zeta, l_1, \ldots, l_j, \Delta_1, \ldots \Delta_j\}$

Table 2: Summary of all cases in the numerical case study

Class of models	Logarithm of the Evidence	Logarithm of the Likelihood factor	Logarithm of the Ockham factor
M_0	8282	8303	-21
M_1	**12837**	12881	-44
M_2	12831	12883	-52

Table 3: Evidence of different classes of models in Case A

Class of models	Logarithm of the Evidence	Logarithm of the Likelihood factor	Logarithm of the Ockham factor
M_0	---	---	---
M_1	**12850**	12880	-30
M_2	12843	12881	-38

Table 4: Evidence of different classes of models in Case B

Class of models	Logarithm of the Evidence	Logarithm of the Likelihood factor	Logarithm of the Ockham factor
M_0	8348	8367	-19
M_1	**12838**	12880	-42
M_2	12833	12882	-49

Table 5: Evidence of different classes of models in Case C

Class of models	Logarithm of the Evidence	Logarithm of the Likelihood factor	Logarithm of the Ockham factor
M_0	8389	8409	-20
M_1	12996	13042	-46
M_2	**13001**	13057	-56
M_3	12995	13059	-64

Table 6: Evidence of different classes of models in Case D

Class of models	Logarithm of the Evidence	Logarithm of the Likelihood factor	Logarithm of the Ockham factor
M_0	12935	12967	-32
M_1	13135	13180	-45
M_2	**13149**	13202	-53
M_3	13144	13205	-61

Table 7: Evidence of different classes of models in Case E

Class of models	Logarithm of the Evidence	Logarithm of the Likelihood factor	Logarithm of the Ockham factor
M_0	8303	8322	-19
M_1	12366	12409	-43
M_2	12864	12923	-59
M_3	**12956**	13020	-64
M_4	12948	13023	-75

Table 8: Evidence of different classes of models in Case F

Case	Crack location l_j (COV %)	Crack extent Δ_j (COV %)	Normalized spring stiffness (COV %)		Damping Ratio ζ (COV %)
			$\tilde{K}_L$	$\tilde{K}_R$	
A	l_1: 0.1797 (1.02)	Δ_1: 0.0520 (5.87)	0.0981 (100.76)	0.2449 (26.65)	0.01 (0.18)
B	l_1: 0.1809 (0.35)	Δ_1: 0.0499 (0.15)	---	---	---
C	l_1: 0.1786 (0.73)	Δ_1: 0.0539 (4.43)	$\tilde{K}$: 0.1884 (12.39)		0.01 (0.18)
D	l_1: 0.1412 (0.69) l_2: 0.0349 (1.33)	Δ_1: 0.0490 (4.16) Δ_2: 0.0283 (14.75)	0.2040 (40.03)	0.3437 (15.87)	0.01 (0.20)
E	l_1: 0.1429 (2.87) l_2: 0.0367 (7.22)	Δ_1: 0.0112 (35.06) Δ_2: 0.0102 (37.64)	0.2060 (55.47)	0.4269 (14.96)	0.01 (0.20)
F	l_1: 0.1406 (5.78) l_2: 0.0393 (1.33) l_3: 0.0802 (1.66)	Δ_1: 0.0494 (17.95) Δ_2: 0.0248 (89.22) Δ_3: 0.0401 (13.72)	0.2145 (97.11)	0.2815 (79.77)	0.01 (0.25)

Table 9: Optimal parameters and the corresponding COV in all cases